

Two-pole structure of the $b_1(1235)$ axial-vector meson

Samson Clymton^{1,*} and Hyun-Chul Kim^{1,2,†}

¹*Department of Physics, Inha University, Incheon 22212, Republic of Korea*

²*School of Physics, Korea Institute for Advanced Study (KIAS), Seoul 02455, Republic of Korea*
(Dated: May 29, 2023)

We investigate the dynamical generation of the b_1 meson in the $\pi\omega$ interaction, using the fully off-mass-shell coupled-channel formalism with the $\pi\omega$, $\eta\rho$, $\pi\phi$, and $K\bar{K}^*$ channels included. We first construct the Feynman amplitudes for the sixteen different kernel amplitudes, considering only the t and u channels. Solving the coupled integral equation, we obtain the transition amplitude for the $\pi\omega$ interaction. We select the axial-vector and isovector channels from the partial-wave expansion and single out the two poles corresponding to the b_1 mesons: $(1306 - i70)$ MeV and $(1356 - i65)$ MeV. They are located below the $K\bar{K}^*$ threshold. The first pole lies below the $\eta\rho$ threshold by about 10 MeV, whereas the second one emerges above it by about 40 MeV. We analyze the effects of the two poles and background contributions to the $\pi\omega$ total cross section by using a toy model.

I. INTRODUCTION

The low-lying pseudoscalar and vector meson octets are believed to be $q\bar{q}$ ground states with quark spins aligned antiparallel (1^1S_0) and parallel (1^3S_1), respectively. The axial-vector mesons are also often considered as orbitally excited $q\bar{q}$ states. For example, there are six different light unflavored axial-vector mesons below 1.5 GeV: $h_1(1170)$, $b_1(1235)$, $a_1(1260)$, $f_1(1285)$, $h_1(1415)$, $f_1(1420)$ [1]. Quark models classify $h_1(1170)$ and $b_1(1235)$ as orbitally excited 1^1P_1 states, and $a_1(1260)$ and $f_1(1285)$ as 1^3P_1 states [2, 3]. However, since all of the axial-vector mesons lie above 1 GeV, a pair of quarks can be created from the vacuum, so that the structure of them may become more complicated. For instance, the $a_1(1260)$ meson can be considered as a molecular state [4–7], which can be dynamically generated in $\pi\rho$ scattering within the coupled-channel formalisms. Since it appears as a resonance below the $K\bar{K}^*$ threshold, it can be regarded as the $K\bar{K}^*$ molecular state [7]. Nagahiro et al. [8] analyzed the compositeness of the a_1 meson and drew a conclusion that it has both the elementary and composite components in comparable amounts.

The $b_1(1235)$ meson can also be dynamically generated as $a_1(1260)$ [5, 6]. In Refs. [5, 6], it was shown that the $b_1(1235)$ is strongly coupled to the $K\bar{K}^*$ channel. Its pole position is located at $(1288 - i28)$ MeV [6]. Experimentally, the $b_1(1235)$ was observed as a $\pi\omega$ resonance at around 1.22 GeV in the $\pi^+p \rightarrow \pi^+ + p + \pi^+ + \pi^- + \pi^0$ process [9]. Its existence was confirmed consecutively [10–19]. In particular, Fukui et al. [17] analyzed the $\pi\omega$ interaction using the partial wave analysis, based on the experimental data on the π^-p charge exchange reaction. In the 1^{+-} wave, they measured respectively the mass and width of the $b_1(1235)$ as $M = (1236 \pm 16)$ MeV and $\Gamma = (151 \pm 31)$ MeV, fitting the intensity of the 1^{+-} wave with the Breit-Wigner form. However, some of the data are off from this form, which may indicate that the structure of the $b_1(1235)$ is not explained by an ordinary P -wave $q\bar{q}$ state.

In the present work, we investigate the $\pi\omega$ interaction within the framework of a fully off-shell coupled-channel formalism. Since the $b_1(1235)$ decays into $\pi\omega$ (seen), $\eta\rho$ (seen), $K\bar{K}^*$ (seen), and $\pi\phi$ ($< 1.5\%$), we consider these decay channels in the current formalism. Constructing all possible kernel amplitudes, we solve the coupled integral equations to derive the transition amplitudes. Unexpectedly, we find two b_1 mesons: $(1306 - i70)$ MeV and $(1356 - i65)$ MeV. The partial-wave ($1^+(1^{+-})$) cross section for $\pi\omega$ scattering resembles that of $\pi\Sigma$ scattering, where $\Lambda(1405)$ reveals a two-pole structure [20, 21]. Albaladejo et al. [22] found the two-pole structure of the $D^*(2400)$ in the light pseudoscalar and D meson interaction in the coupled-channel formalism (see a recent review [23] for detailed discussion on the two-pole structures). Moreover, there is a peculiar fact concerning the b_1 meson. In contrast to all other axial-vector mesons, there is no excited state for the b_1 meson. For example, we have two excited a_1 mesons such as $a_1(1420)$ and $a_1(1640)$, $f_1(1420)$ and $f_1(1510)$ for the f_1 meson, and $h_1(1415)$ and $h_1(1595)$ for the h_1 below 2 GeV. Even in the strange channel, we have two excited states $K_1(1400)$ and $K_1(1650)$ for the $K_1(1270)$ [1]. Thus, the two-pole structure of the b_1 meson may give a clue in understanding the reason why the excited b_1 mesons have not been found.

The current work is organized as follows: In the next section, we introduce the fully off-shell coupled-channel formalism. The transition kernel potentials are constructed by using the effective Lagrangian. Incorporating them in the coupled integral equations, we derive the transition amplitudes for the $\pi\omega$ interaction. In Sect. III, We carry out the partial-wave expansion to get the $1^+(1^{+-})$ channel corresponding to the b_1 meson. We compare the total cross

* E-mail: sclymton@inha.edu

† E-mail: hchkim@inha.ac.kr

section for $\pi\omega$ scattering in the $1^+(1^{+-})$ channel with the data [17]. We pin down the two poles for the b_1 in the T matrix in the complex plane. We construct a toy model including the two b_1 mesons to compare the results with those from the current work and data. In the last section, we summarize the current work and draw conclusions.

II. COUPLED CHANNEL FORMALISM

The scattering amplitude is defined as

$$\mathcal{S}_{fi} = \delta_{fi} - i(2\pi)^4 \delta(P_f - P_i) \mathcal{T}_{fi}, \quad (1)$$

where P_i and P_f stand for the total four momenta of the initial and final states. The transition amplitude \mathcal{T}_{fi} can be derived from the Bethe-Salpeter integral equation

$$\mathcal{T}_{fi}(p', p; s) = \mathcal{V}_{fi}(p', p; s) + \frac{1}{(2\pi)^4} \sum_k \int d^4 q \mathcal{V}_{fk}(p', q; s) \mathcal{G}_k(q; s) \mathcal{T}_{ki}(q, p; s), \quad (2)$$

where p and p' denote the relative four-momentum of the initial and final states, respectively. q is the off-mass-shell momentum for the intermediate states in the center of momentum frame. s represents the square of the total energy, which is just one of the Mandelstam variables, $s = P_i^2 = P_f^2$. The coupled integral equation given in Eq. (2) can be depicted as in Fig. 1. To avoid the complexity due to the four-dimensional integral equation, we make a three-

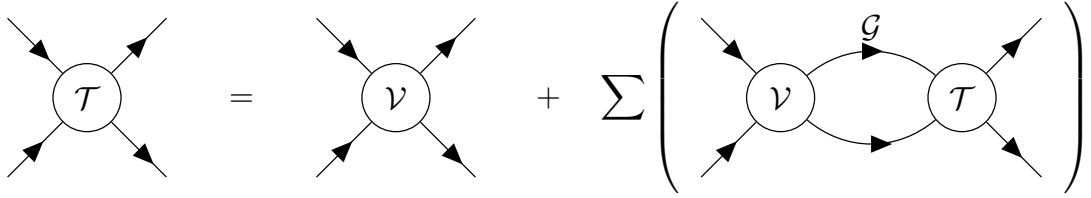


FIG. 1. Graphical representation of the coupled integral scattering equation.

dimensional reduction. While there are several different methods for the three-dimensional reduction, we take the Blankenbecler-Sugar scheme [24, 25], which takes the two-body propagator in the form of

$$\mathcal{G}_k(q) = \delta \left(q_0 - \frac{E_{k1}(\mathbf{q}) - E_{k2}(\mathbf{q})}{2} \right) \frac{\pi}{E_{k1}(\mathbf{q}) E_{k2}(\mathbf{q})} \frac{E_k(\mathbf{q})}{s - E_k^2(\mathbf{q})}, \quad (3)$$

where E_k represents the total on-mass-shell energy of the intermediate state, $E_k = E_{k1} + E_{k2}$, and \mathbf{q} denote the three-momenta of the intermediate state. Utilizing Eq. (3), we obtain the following coupled integral equation

$$\mathcal{T}_{fi}(\mathbf{p}', \mathbf{p}) = \mathcal{V}_{fi}(\mathbf{p}', \mathbf{p}) + \frac{1}{(2\pi)^3} \sum_k \int \frac{d^3 q}{2E_{k1}(\mathbf{q}) E_{k2}(\mathbf{q})} \mathcal{V}_{fk}(\mathbf{p}', \mathbf{q}) \frac{E_k(\mathbf{q})}{s - E_k^2(\mathbf{q})} \mathcal{T}_{ki}(\mathbf{q}, \mathbf{p}), \quad (4)$$

where \mathbf{p} and \mathbf{p}' are the relative three-momenta of the initial and final states in the center of momentum frame, respectively.

We first construct the kernel amplitudes in Eq. (4) by computing the tree-level Born diagrams, where the initial and final states are given in terms of the pseudoscalar and vector mesons, as illustrated in Fig. 2. Note that we do not include any pole diagrams in the s channel. The effective Lagrangians describe the interacting vertices given in Fig. 2. They are given as

$$\begin{aligned} \mathcal{L}_{PPV} &= \sqrt{2} g_{PPV} \text{Tr}([P, \partial_\mu P] V^\mu), \\ \mathcal{L}_{VVV} &= -\sqrt{2} g_{VVV} \text{Tr}((\partial_\mu V_\nu - \partial_\nu V_\mu) V^\mu V^\nu), \\ \mathcal{L}_{PVV} &= \sqrt{2} \frac{g_{PVV}}{m_V} \varepsilon^{\mu\nu\alpha\beta} \text{Tr}(\partial_\mu V_\nu \partial_\alpha V_\beta P). \end{aligned} \quad (5)$$

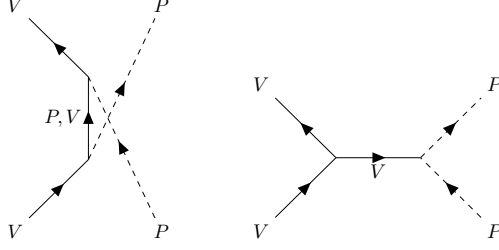


FIG. 2. u - and t -channel diagrams for the meson-exchanged diagrams are depicted in the left and right panels, respectively. P and V stand for the pseudoscalar and vector mesons.

Here, P and V denote the SU(3) matrices for the pseudoscalar and vector meson octets, respectively

$$P = \begin{pmatrix} \frac{1}{\sqrt{2}}\pi^0 + \frac{1}{\sqrt{6}}\eta & \pi^+ & K^+ \\ \pi^- & -\frac{1}{\sqrt{2}}\pi^0 + \frac{1}{\sqrt{6}}\eta & K^0 \\ K^- & \bar{K}^0 & -\frac{2}{\sqrt{6}}\eta \end{pmatrix}, \quad V = \begin{pmatrix} \frac{1}{\sqrt{2}}\rho_\mu^0 + \frac{1}{\sqrt{2}}\omega_\mu & \rho_\mu^+ & K_\mu^{*+} \\ \rho_\mu^- & -\frac{1}{\sqrt{2}}\rho_\mu^0 + \frac{1}{\sqrt{2}}\omega_\mu & K_\mu^{*0} \\ K_\mu^{*-} & \bar{K}_\mu^{*0} & \phi_\mu \end{pmatrix}. \quad (6)$$

Note that we consider the ideal mixing for the vector nonet, while treating η_8 as the physical η meson for the pseudoscalar octet. We regard the ρ meson as a gauge vector meson in the hidden local symmetry [26, 27]. Thus, the coupling constants in the first two Lagrangians were identical, while the last one was related to the anomaly term explaining the ω decays into $\pi\rho$. We adopt the value of the coupling constant from Ref. [28], which is given as $g_{\pi\pi\rho}^2/4\pi = 2.84$ and $(g_{\pi\rho\omega}^2/4\pi)m_\omega^2 = 7.5$, which can be related to the coupling constant in Eq. (5) by the SU(3) symmetric factor: $g_{\pi\pi\rho} = 2g_{PPV}$ and $g_{\pi\rho\omega}m_\omega = 2g_{PVV}$. We assume that the SU(3) symmetry is respected, except for the ϕ coupling, which we allow to vary by approximately 1 %.

The Born amplitudes in the t - and u -channels can be expressed in terms of three different types of amplitudes:

$$\mathcal{A}_P^u(\mathbf{p}', \mathbf{p}) = -\text{IS } g_{PPV}^2 F^2(u) (2p_2 - p_3) \cdot \epsilon^* \mathcal{P}(p_1 - p_4) (2p_4 - p_1) \cdot \epsilon, \quad (7)$$

$$\mathcal{A}_V^u(\mathbf{p}', \mathbf{p}) = -\text{IS } \frac{g_{PVV}^2}{m_V^2} F^2(u) \varepsilon_{\mu\nu\alpha\beta} p_3^\mu \epsilon^{*\nu} (p_3 - p_2)^\alpha \mathcal{P}^{\beta\delta} (p_1 - p_4) \varepsilon_{\gamma\sigma\eta\delta} p_1^\gamma \epsilon^\sigma (p_1 - p_4)^\eta, \quad (8)$$

$$\mathcal{A}_V^t(\mathbf{p}', \mathbf{p}) = -\text{IS } g_{PPV}^2 F^2(t) (p_2 + p_4)^\mu \mathcal{P}_{\mu\nu}(p_1 - p_3) [(2p_1 - p_3) \cdot \epsilon^* \epsilon^\nu + (2p_3 - p_1) \cdot \epsilon \epsilon^{*\nu} - \epsilon \cdot \epsilon^* (p_1 + p_3)^\nu]. \quad (9)$$

The first two amplitudes represent pseudoscalar- and vector-meson exchanges in the u -channel, while the last one represents vector-meson exchange in the t -channel. The flavor components of Eq. (5) can be evaluated in the isospin bases and yield factors labeled as IS. The polarization vectors of the incoming and outgoing vector particles are labeled as ϵ and ϵ^* , respectively. The four-momenta of the particles involved are given as follows:

$$\begin{aligned} p_1 &= (E_{1,\text{off}}, \mathbf{p}), & p_2 &= (E_{2,\text{off}}, -\mathbf{p}), \\ p_3 &= (E_{3,\text{off}}, \mathbf{p}'), & p_4 &= (E_{4,\text{off}}, -\mathbf{p}'). \end{aligned} \quad (10)$$

Following the BbS scheme, the off-shell energies of the particle are written [25] as

$$\begin{aligned} E_{1,\text{off}} &= \frac{1}{2} (\sqrt{s} + E_1(\mathbf{p}) - E_2(\mathbf{p})), & E_{2,\text{off}} &= \frac{1}{2} (\sqrt{s} + E_2(\mathbf{p}) - E_1(\mathbf{p})), \\ E_{3,\text{off}} &= \frac{1}{2} (\sqrt{s} + E_3(\mathbf{p}') - E_4(\mathbf{p}')), & E_{4,\text{off}} &= \frac{1}{2} (\sqrt{s} + E_4(\mathbf{p}') - E_3(\mathbf{p}')), \end{aligned} \quad (11)$$

where they will satisfy the on-shell energy condition when $E_1(\mathbf{p}) + E_2(\mathbf{p}) = E_3(\mathbf{p}') + E_4(\mathbf{p}') = \sqrt{s}$. The propagators for the spin-0 and spin-1 mesons are expressed by

$$\mathcal{P}(p) = \frac{1}{p^2 - m^2}, \quad \mathcal{P}_{\mu\nu}(p) = \frac{1}{p^2 - m^2} \left(-g_{\mu\nu} + \frac{p_\mu p_\nu}{m^2} \right), \quad (12)$$

where the m are the corresponding exchange masses. As in the previous study [7], the energy-dependent terms in the denominator of the propagator are turned off.

Since the hadrons have finite sizes, we introduce a form factor at each vertex. We use the following parametrization for the form factors

$$F(t) = \left(\frac{n\Lambda^2 - m^2}{n\Lambda^2 - t} \right)^n, \quad F(u) = \left(\frac{n\Lambda^2 - m^2}{n\Lambda^2 - u} \right)^n, \quad (13)$$

where n is determined by the power of the momentum in the vertex. While the cut-off masses Λ in Eq. (13) are free parameters, we take a strategy to reduce the uncertainties associated with their values. We add a fixed amount of (500 – 700) MeV to the corresponding mass of the exchange meson, motivated by the fact that a heavier particle typically has a smaller size, as indicated in Refs. [29, 30]. Consequently, we have set the value of Λ to be larger than the corresponding meson mass by around (500 – 700) MeV. To fit the data, however, we choose a larger value of the cut-off mass for some exchanged particles (see Table I). Moreover, for simplicity, we neglect the energy and angular dependence of the form factors as done in Ref. [28].

As mentioned in the introduction, the b_1 axial-vector meson has the following decay channels: $\pi\omega$, $\pi\phi$, $\eta\rho$, and $K\bar{K}^*$ with the positive G -parity. Thus, we consider these four different channels in the the potential matrix \mathcal{V} as follows:

$$\mathcal{V} = \begin{pmatrix} \mathcal{V}_{\pi\omega \rightarrow \pi\omega} & \mathcal{V}_{\pi\phi \rightarrow \pi\omega} & \mathcal{V}_{\eta\rho \rightarrow \pi\omega} & \mathcal{V}_{K\bar{K}^* \rightarrow \pi\omega} \\ \mathcal{V}_{\pi\omega \rightarrow \pi\phi} & \mathcal{V}_{\pi\phi \rightarrow \pi\phi} & \mathcal{V}_{\eta\rho \rightarrow \pi\phi} & \mathcal{V}_{K\bar{K}^* \rightarrow \pi\phi} \\ \mathcal{V}_{\pi\omega \rightarrow \eta\rho} & \mathcal{V}_{\pi\phi \rightarrow \eta\rho} & \mathcal{V}_{\eta\rho \rightarrow \eta\rho} & \mathcal{V}_{K\bar{K}^* \rightarrow \eta\rho} \\ \mathcal{V}_{\pi\omega \rightarrow K\bar{K}^*} & \mathcal{V}_{\pi\phi \rightarrow K\bar{K}^*} & \mathcal{V}_{\eta\rho \rightarrow K\bar{K}^*} & \mathcal{V}_{K\bar{K}^* \rightarrow K\bar{K}^*} \end{pmatrix}. \quad (14)$$

Each component of the potential matrix can be constructed by computing the tree-level Born diagrams with one-meson exchanges, which are listed in Table I along with the corresponding IS factors and cutoff parameters required for the calculation of the potential, as given in Eqs.(7)-(9).

TABLE I. The isospin times SU(3) factor (IS) and cutoff parameter (Λ) in MeV for possible exchange diagrams for each reaction. m is the exchange mass.

Reaction	Exchange	Type	IS	$\Lambda - m$
$\pi\omega \rightarrow \pi\omega$	ρ	u	4	1200
$\pi\omega \rightarrow \eta\rho$	ω	u	$4/\sqrt{3}$	1000
$\pi\omega \rightarrow K\bar{K}^*$	K	u	$\sqrt{2}$	600
	K^*	t	$\sqrt{2}$	1150
$\pi\phi \rightarrow K\bar{K}^*$	K	u	-2	600
	K^*	t	-2	800
$\eta\rho \rightarrow \eta\rho$	ρ	u	$4/3$	830
$\eta\rho \rightarrow K\bar{K}^*$	K	u	$\sqrt{6}$	600
	K^*	t	$\sqrt{6}$	1050
$K\bar{K}^* \rightarrow K\bar{K}^*$	ρ	t	1	600
	ω	t	-1	600
	ϕ	t	-2	1400
$K\bar{K}^* \rightarrow \bar{K}K^*$	π	u	1	600
	η	u	-3	600
	ρ	u	-1	600
	ω	u	1	600
	ϕ	u	2	1400

In Fig. 3, we show the numerical results for the on-shell potentials. Note that channels without a tree-level amplitude have been omitted from Fig. 3. Analysis of Fig. 3 and Table I reveals that the $\mathcal{V}_{\pi\omega \rightarrow \eta\rho}$ potential, which contains a single u exchange diagram, is significantly smaller than the $\mathcal{V}_{\pi\omega \rightarrow K\bar{K}^*}$ potential, which contains u - and t - exchange diagram, even though the former has an IS factor more than twice as large as the latter. This discrepancy suggests that the t -exchange diagram is considerably stronger than the u -exchange diagram. Consequently, we observe in Fig. 3 that all channels with $K\bar{K}^*$ as the initial or final state produce larger values of the potential due to the presence of the t -exchange diagram. In particular, the $\mathcal{V}_{\eta\rho \rightarrow K\bar{K}^*}$ has the strongest contribution due to its large IS factor. Although $\mathcal{V}_{K\bar{K}^* \rightarrow K\bar{K}^*}$ has the three t -exchange diagrams, the ρ and ω exchanges cancel each other because of the different sign of the IS factor, leaving only the ϕ exchange contribution, which has a smaller IS factor than that of K^* exchange in the $\eta\rho \rightarrow K\bar{K}^*$ process. These results clearly indicate that the $K\bar{K}^*$ channel is crucial in generating the resonances dynamically within the current framework. Similar conclusions are found in Refs. [5, 6].

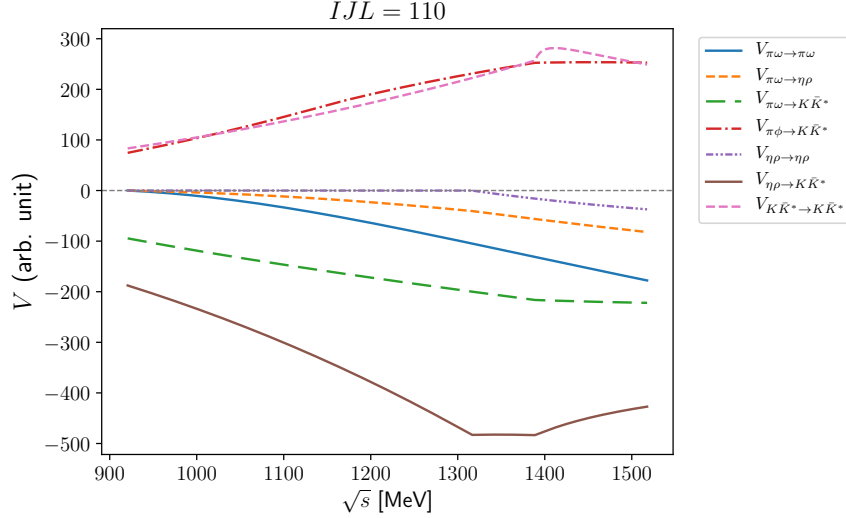


FIG. 3. Numerical results for the transition potentials in seven different channels as functions of the total energy.

To focus on the b_1 meson, we need to carry out the partial-wave expansion of the \mathcal{V} and \mathcal{T} matrices, resulting in a one-dimensional integral equation given by

$$\mathcal{T}_{\lambda'\lambda}^{J(fi)}(\mathbf{p}', \mathbf{p}) = \mathcal{V}_{\lambda'\lambda}^{J(fi)}(\mathbf{p}', \mathbf{p}) + \frac{1}{(2\pi)^3} \sum_{k, \lambda_k} \int \frac{q^2 dq}{2E_{k1}E_{k2}} \mathcal{V}_{\lambda'\lambda_k}^{J(fk)}(\mathbf{p}', \mathbf{q}) \frac{E_k}{s - E_k^2} \mathcal{T}_{\lambda_k\lambda}^{J(ki)}(\mathbf{q}, \mathbf{p}), \quad (15)$$

where λ' , λ and λ_k denote the helicities of the final (f), initial (i) and intermediate (k) states, respectively. The partial-wave \mathcal{V} amplitudes can be expressed as

$$\mathcal{V}_{\lambda'\lambda}^{J(fi)}(\mathbf{p}', \mathbf{p}) = 2\pi \int d(\cos\theta) d_{\lambda'\lambda}^J(\theta) \mathcal{V}_{\lambda'\lambda}^{fi}(\mathbf{p}', \mathbf{p}, \theta), \quad (16)$$

where θ denote the scattering angle and $d_{\lambda'\lambda}^J(\theta)$ stand for the matrix elements of the Wigner D functions in the helicity basis. The partial-wave \mathcal{T} amplitudes are expressed in a similar way.

The integral equation presented in Eq. (15) contains the singularity originating from the two-body meson propagator \mathcal{G} . To regulate this singularity, we isolate the singular part of the propagator. The resulting regularized integral equation is given by

$$\mathcal{T}_{\lambda'\lambda}^{fi}(\mathbf{p}', \mathbf{p}) = \mathcal{V}_{\lambda'\lambda}^{fi}(\mathbf{p}', \mathbf{p}) + \frac{1}{(2\pi)^3} \sum_{k, \lambda_k} \left[\int_0^\infty dq \frac{qE_k}{E_{k1}E_{k2}} \frac{\mathcal{F}(q) - \mathcal{F}(\tilde{q}_k)}{s - E_k^2} + \frac{1}{2\sqrt{s}} \left(\ln \left| \frac{\sqrt{s} - E_k^{\text{thr}}}{\sqrt{s} + E_k^{\text{thr}}} \right| - i\pi \right) \mathcal{F}(\tilde{q}_k) \right], \quad (17)$$

with

$$\mathcal{F}(q) = \frac{1}{2} q \mathcal{V}_{\lambda'\lambda_k}^{fk}(\mathbf{p}', \mathbf{q}) \mathcal{T}_{\lambda_k\lambda}^{ki}(\mathbf{q}, \mathbf{p}). \quad (18)$$

and \tilde{q}_k is the momentum when $E_{k1} + E_{k2} = \sqrt{s}$. The regularization is applied only when the total energy \sqrt{s} exceeds the threshold energy of the k -th channel E_k^{thr} . It is worth noting that the form factor that was introduced in the \mathcal{V} amplitudes provides sufficient suppression in the high-momentum region, thus allowing for the regularization of the integration.

To obtain \mathcal{T} from Eq. (17) numerically, we expand the \mathcal{V} matrix in the helicity states and momentum space, where the momenta are obtained by using the Gaussian quadrature method. We then derive the \mathcal{T} matrix by using the Haftel-Tabakin method for the matrix inversion [31], namely

$$\mathcal{T} = \left(1 - \mathcal{V}\tilde{\mathcal{G}} \right)^{-1} \mathcal{V}. \quad (19)$$

Note that the \mathcal{T} matrix is still in the helicity basis. To facilitate the analysis, we express the \mathcal{T} matrix in the IJL particle basis [32]. The relations between the \mathcal{T} matrix elements in the two bases are given by

$$\mathcal{T}_{J,J}^J = \mathcal{T}_{++}^J - \mathcal{T}_{+-}^J, \quad (20)$$

$$\mathcal{T}_{J-1,J-1}^J = \frac{1}{\sqrt{2J+1}} \left[J\mathcal{T}_{00}^J + (J+1)(\mathcal{T}_{++}^J + \mathcal{T}_{+-}^J) + \sqrt{2J(J+1)}(\mathcal{T}_{+0}^J + \mathcal{T}_{0+}^J) \right], \quad (21)$$

$$\mathcal{T}_{J+1,J+1}^J = \frac{1}{\sqrt{2J+1}} \left[(J+1)\mathcal{T}_{00}^J + J(\mathcal{T}_{++}^J + \mathcal{T}_{+-}^J) - \sqrt{2J(J+1)}(\mathcal{T}_{+0}^J + \mathcal{T}_{0+}^J) \right], \quad (22)$$

where we have only shown the diagonal part of $\mathcal{T}_{L,L}^J$ as it is relevant to the particle production. Here, we define \mathcal{T}_{IJL} to be the component of the \mathcal{T} matrix in the particle basis for a given total isospin I , total angular momentum J , and orbital angular momentum L .

III. RESULTS AND DISCUSSIONS

A. The b_1 meson

The existence of the b_1 meson is supported by experimental observations in pion-proton scattering [17, 18], proton-antiproton annihilation [19], and photoproduction [15]. However, these hadronic reactions are known to be sensitive to hadronic backgrounds, which causes significant uncertainties into the data. Thus, as an alternative process, the τ decay was considered as a pristine one for studying the axial vector meson. In contrast to the a_1 meson, however, the b_1 meson in the τ decay has not yet been conclusively identified. Efforts have been made to study the b_1 meson in the $\tau \rightarrow \pi\omega\nu_\tau$ decay, but the dominance of the first-class ρ -meson vector current in the decay makes it difficult to discern the b_1 meson [33]. Thus, one has to rely on hadronic reactions to examine the properties of the b_1 meson. In the current work, we will consider $\pi\omega$ scattering arising from the charge-exchange $\pi\rho \rightarrow \omega\pi n$ reaction to investigate the b_1 meson, specifically taking the experimental data [17] into account.

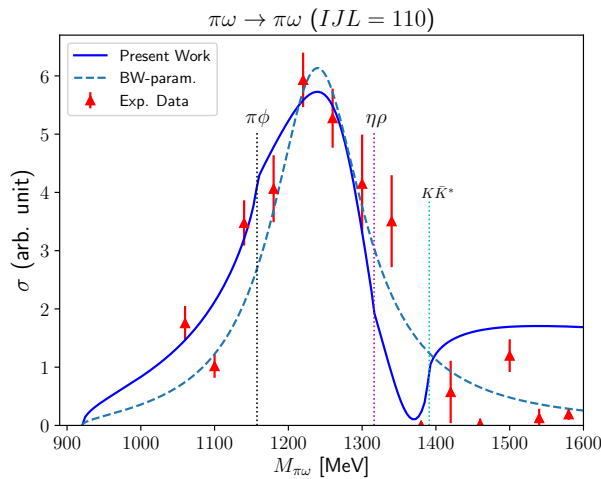


FIG. 4. The $\pi\omega \rightarrow \pi\omega$ total cross section for $IJL = 110$ as a function of $\pi\omega$ invariant mass. The experimental data are taken from Ref. [17].

We conduct the numerical computation of the invariant mass distribution for the charge-exchange reaction, comparing the current results with the experimental data [17]. We adjust the cutoff masses as little as possible, while keeping all other parameters the same as those determined in the previous study of the $a_1(1260)$ meson [7]. To describe the experimental data, we assume that the total cross section in arbitrary unit is proportional to the $\pi\omega$ elastic \mathcal{T} amplitude with a constant factor C , expressed as

$$\sigma \equiv -C \text{Im}[\mathcal{T}_{\pi\omega}(M_{\pi\omega})]. \quad (23)$$

The resonance structure is generally sensitive to the cutoff masses. It is understandable, given the fact that the singularities generated dynamically in the current work arise from the off-shell contribution to the \mathcal{T} matrix. In the

course of the fitting process, we keep the cutoff masses to be $\Lambda = m + 600$ MeV as far as possible, where m is the mass of the exchange particle. By doing that we can suppress numerical uncertainties. However, we have found that $\Lambda = 1.4$ GeV should be used for the ϕ -exchange diagram (see Table I). The results are in good agreement with the experimental data, as demonstrated in Fig. 4. We observe that the total cross section falls off drastically till the $K\bar{K}^*$ threshold, which is a typical threshold behavior. Interestingly, the experimental data also exhibits a similar tendency. We compare the present result with the single resonance structure coming from the Breit-Wigner form [17]

$$\sigma = \rho(M_{\pi\omega}) \left| \frac{g^2}{M_{\pi\omega}^2 - M^2 + iM\Gamma} \right|^2, \quad (24)$$

where the mass and width are taken to be experimental values $M = 1236$ MeV and $\Gamma = 151$ MeV, respectively. The phase space factor is given by $\rho = |\mathbf{p}|/8\pi M_{\pi\omega}$, where \mathbf{p} is the three-momentum of the particle in the CM frame. The BW form produces the experimental data near the resonance region well, whereas it cannot explain the threshold behavior near the $K\bar{K}^*$ threshold, which implies that the coupled-channel effects are required.

In order to investigate the properties of the $b_1(1235)$ meson, we search for the singularities in the \mathcal{T} matrix in the complex energy plane. The resulting pole position of $\sqrt{s_R} = (1306 - i70)$ MeV, which corresponds to the width of 140 MeV, is consistent with both experimental data [17] and the average value provided by the PDG. In contrast, recent lattice calculations [34] yielded a pole position for the b_1 meson at $[(1382 \pm 15) - i(46 \pm 15)]$ MeV, where the $\pi\omega$ and $\pi\phi$ scattering channels were coupled. Meanwhile, the chiral unitary model [6] obtained a pole position at $(1247 - i28)$ MeV for the b_1 meson. Both the works underestimate the width of the b_1 meson.

B. Two-pole structure of b_1 meson

As mentioned previously, we have searched for the singularities of the \mathcal{T} matrix in the complex energy plane. In addition to the first pole $\sqrt{s_R} = (1306 - i70)$ MeV, we also find the second pole at $(1356 - i65)$ MeV. To show these two poles, we present a contour plot of the $\mathcal{T}_{\pi\omega \rightarrow \pi\omega}(IJL = 110)$ amplitude as a function of the complex energy in the second Riemann sheet. Figure 5 displays the distinct two poles. The first pole appears below the $\eta\rho$ threshold, whereas the second pole comes out between the $\eta\rho$ and $K\bar{K}^*$ thresholds. Specifically, the first pole lies below the $\eta\rho$ threshold by about 10 MeV, while the second pole emerges above it by about 40 MeV and below the $K\bar{K}^*$ threshold by about 30 MeV. The widths of the two b_1 mesons are comparable each other.

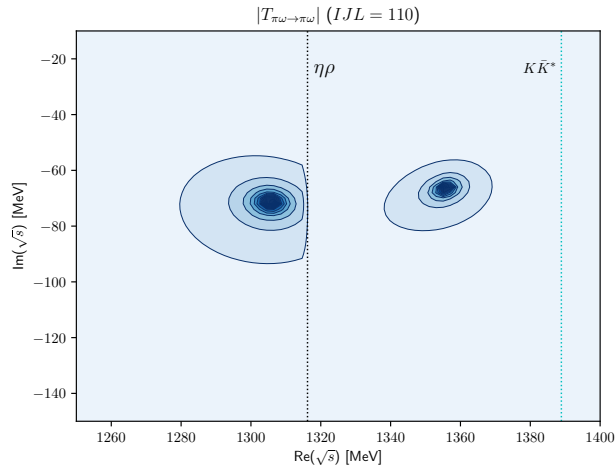


FIG. 5. The $\pi\omega \rightarrow \pi\omega$ total cross section for $IJL = 110$ as a function of $\pi\omega$ invariant mass. The experimental data are taken from Ref. [17].

To better understand the properties of the b_1 mesons, it is of great use to calculate the coupling strengths of the $b_1(1235)$ resonances, which can be derived from the residues of the \mathcal{T} matrix:

$$\mathcal{R}_{a,b} = \lim_{s \rightarrow s_R} (s - s_R) \mathcal{T}_{a,b}/4\pi, \quad (25)$$

$$g_a = \sqrt{\mathcal{R}_{a,a}}, \quad (26)$$

Note that, since we define the coupling strengths in this way, their signs cannot be determined. The results for the coupling strengths are listed in Table II. As shown in it, the S -wave $K\bar{K}^*$ channel is the most strongly coupled to both the poles: $g_{K\bar{K}^*} = (8.64 + i0.34)$ GeV and $g_{K\bar{K}^*} = (8.30 + i2.78)$ GeV for the first and second poles, respectively. Interestingly, the first pole for the b_1 meson has a larger value of the $\eta\rho$ coupling strength than the second one. It is understandable, since the first pole is closer to the $\eta\rho$ threshold, compared to the second one. The first pole is also more strongly coupled to the $\pi\omega$ and $\pi\phi$ channels. However, we want to mention that it is essential to include all channels so that the b_1 resonances can be generated dynamically. It is also interesting to compute the ratios of the D - to S -wave amplitudes in decays of the b_1 mesons to each channel. In Table III, we list the results for them. In particular, we derive the value of 0.36 for the first pole, and 0.40 for the second pole. The experimental data on the D/S ratio is given as 0.277 ± 0.027 . Since we have two poles for the b_1 meson, we cannot directly compare the results with the experimental value. The D/S ratios for all other channels are generally very small. The D/S ratios for the

TABLE II. Coupling strength in unit of GeV of the b_1 resonance to the S and D wave states in the four different channels.

$\sqrt{s_R}$ [MeV]	1306 - $i70$	1356 - $i65$
$g_{\pi\omega}(S\text{-wave})$	$3.07 + i2.14$	$0.68 + i2.91$
$g_{\pi\omega}(D\text{-wave})$	$1.33 + i0.29$	$0.84 + i0.87$
$g_{\pi\phi}(S\text{-wave})$	$2.34 + i1.35$	$0.84 + i1.84$
$g_{\pi\phi}(D\text{-wave})$	$0.20 - i0.03$	$0.19 + i0.11$
$g_{\eta\rho}(S\text{-wave})$	$3.36 + i1.91$	$0.54 + i3.16$
$g_{\eta\rho}(D\text{-wave})$	$0.03 - i0.08$	$0.48 - i0.06$
$g_{K\bar{K}^*}(S\text{-wave})$	$8.64 + i0.34$	$8.30 + i2.78$
$g_{K\bar{K}^*}(D\text{-wave})$	$0.18 + i0.17$	$0.02 + i0.17$

TABLE III. D/S amplitude ratios of the b_1 resonance in the four different decay channels, obtained from the ratio of the absolute value of the coupling strength of the b_1 to the D and S wave states.

Pole	Channels				
	$\pi\omega$	$\pi\phi$	$\eta\rho$	$K\bar{K}^*$	
1306 - $i70$ MeV	0.36	0.07	0.02	0.03	
1356 - $i65$ MeV	0.40	0.11	0.15	0.02	

second pole in the decays of $\pi\phi$ and $\eta\rho$ are about 10 %.

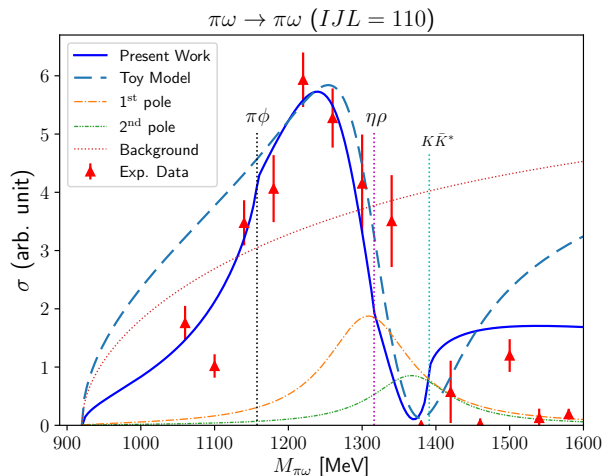


FIG. 6. The $\pi\omega \rightarrow \pi\omega$ total cross section for $IJL = 110$ as a function of $\pi\omega$ invariant mass. The experimental data are taken from Ref. [17].

To get a clearer picture of the two-pole structure of the b_1 meson and the effect of the phase of the coupling strengths, we propose a toy model that includes the two poles in the Breit-Wigner form. To describe the experimental data [17], we need to introduce the background amplitude. So, the T amplitude in the toy model is constructed as

follows:

$$T(s) = T_{\text{pole}}(s) + T_{\text{back}}(s) \quad (27)$$

where the pole part of the T amplitude contains two resonances corresponding to those found in the current work. They are parametrized by the Breit-Wigner form

$$\frac{g_{\pi\omega b_1}^2}{m^2 - s - im\Gamma} \quad (28)$$

where the masses, widths, and coupling strengths to the $\pi\omega$ channel are taken from Table II. The T_{back} stands for the constant background T amplitude, which is introduced to fit the data. The total cross section is then obtained as

$$\sigma(s) = f\rho(s)|T(s)|^2 = f \frac{|\mathbf{p}|}{8\pi\sqrt{s}} |T(s)|^2 \quad (29)$$

where \mathbf{p} is the momentum of ω in the CM frame and the factor f is introduced to fit the experimental data. In Fig. 6, we draw the results from the toy model. The dot-dashed and dot-dot-dashed curves depict the first and second resonances for the b_1 mesons, respectively, whereas the dotted one displays the background contribution. Note that the $M_{\pi\omega}$ dependence of the background contribution arises from the phase-space factor. The long dashed curve shows the total result given by Eq. (27), which describes the experimental data in the vicinity of the resonance region relatively well. Note that it deviates from the data below the $\pi\phi$ and above the $K\bar{K}^*$ thresholds, because the toy model aims only at the resonance region. It implies that the two poles can describe the apparent resonance of the known $b_1(1235)$ meson. The $b_1(1235)$ arises from the constructive interference of the first pole and the background contribution. On the other hand, the threshold behavior is governed by the destructive interference of all the contributions. In particular, the second pole comes into essential play in explaining the threshold behavior.

Actually, the two-pole structure in hadron spectroscopy is not a novel observation [23]. For example, the $\Lambda(1405)$ appears from the two Λ poles, i.e. $\Lambda(1380)$ and $\Lambda(1405)$ [1], which was initially found in Ref. [20], where the K^-p interaction was examined in a chiral unitary approach [20] with the $\pi\Sigma$, $\eta\Lambda$ and $K\Xi$ channels coupled. A further study [21] demonstrated that, owing to the phase difference between the two poles, only a single resonance was observed experimentally. In addition, the same approach uncovered the two-pole structure in the heavy meson domain [35]: the excited D and B mesons with quantum numbers $J^P = 0^+$ and 1^+ originate from the two-pole resonances. The $K_1(1270)$ meson in the light-meson sector were also considered to have the two-pole structures [6, 36]. Notably, the two-pole structure cannot easily be separated by experiments, and thus experimental observations always led to a single resonance¹. The $b_1(1235)$ may also be the case. In particular, the behavior of the total cross section near the $K\bar{K}^*$ threshold holds the significant clue about the fact that the $b_1(1235)$ originates from the two b_1 mesons, $b_1(1306)$ and $b_1(1356)$.

Finally, we want to discuss the coupling strengths of the two b_1 mesons. The results are given respectively as $g_{\pi\omega} = (3.07 + i2.14)$ GeV and $g_{\pi\omega} = (0.68 + i2.91)$ GeV for the first and second b_1 mesons, as listed in Table II. In particular, the coupling strength of the second pole has the larger imaginary part than its real one. This finding is similar to the case of the $\Lambda(1405)$ [21], where the coupling strength to the $\pi\Sigma$ channel of the higher energy pole of $\Lambda(1405)$ has the stronger imaginary part, resulting in a threshold behavior near the $\bar{K}N$ threshold in $\pi\Sigma$ elastic scattering.

IV. SUMMARY AND CONCLUSION

In the current work, we aimed at investigating the b_1 meson in $\pi\omega$ scattering within the framework of the fully off-mass-shell coupled-channel formalism. Since the b_1 meson has the four decay modes, we considered the corresponding channels, i.e., $\pi\omega$, $\eta\rho$, $K\bar{K}^*$, and $\pi\phi$. We first constructed the tree-level kernel amplitudes with all possible transitions, using the effective Lagrangians with flavor SU(3) symmetry and hidden local gauge symmetry for the vector mesons. We introduced the form factors at each vertex. Using the kernel amplitudes, we solved the fully off-mass-shell Blankenbecler-Sugar coupled integral equation. Since we are interested in the b_1 channel, we performed the partial-wave expansion to select the partial wave with $I = 1$, $J = 1$, and $L = 0$, which corresponds to the b_1 channel. We compared the numerical results for the total cross section with the experimental data. The results describe the $b_1(1235)$ resonance very well. They also reveal the threshold behavior in the vicinity of the $K\bar{K}^*$ channel. We

¹ Note that $\Lambda(1380)$ and $\Lambda(1405)$ could be distinguished by the proton electroproduction [37].

scanned the transition amplitude for the $\pi\omega$ interaction in the complex energy plane, we found the positions of the two singularities: the one is located below the $\eta\rho$ threshold, whereas the other is positioned above the $\eta\rho$ and below the $K\bar{K}^*$ thresholds. We also extracted the coupling strengths of the b_1 coupled to the four different channels in both the S and D waves. To analyze the two-pole structure, we constructed the toy model that contains the pole amplitudes for the two b_1 mesons in the Breit-Wigner form and the background contributions. We observed that the $b_1(1235)$ resonance appears from the constructive interference of the first b_1 and background contribution whereas the threshold behavior near the $K\bar{K}^*$ threshold arises from the destructive interference of all the contributions. Specifically, the second pole plays a critical role in describing the threshold behavior of the total cross section. We concluded that the $b_1(1235)$ meson occurs from the two b_1 mesons, i.e., $b_1(1306)$ and $b_1(1356)$.

ACKNOWLEDGMENTS

We are grateful to Jung-Keun Ahn, Tetsuo Hyodo, Hee-Jin Kim, and Seung-il Nam for fruitful discussions. The present work was supported by Inha University Grant, 2023.

-
- [1] R. L. W. et al. (Particle Data Group), *Prog. Theor. Exp. Phys.* **2022**, 083C01 (2022).
 - [2] S. Godfrey and N. Isgur, *Phys. Rev. D* **32**, 189 (1985).
 - [3] D. Ebert, R. N. Faustov, and V. O. Galkin, *Phys. Rev. D* **79**, 114029 (2009), arXiv:0903.5183 [hep-ph].
 - [4] J. L. Basdevant and E. L. Berger, *Phys. Rev. D* **16**, 657 (1977).
 - [5] M. F. M. Lutz and E. E. Kolomeitsev, *Nucl. Phys. A* **730**, 392 (2004), arXiv:nucl-th/0307039.
 - [6] L. Roca, E. Oset, and J. Singh, *Phys. Rev. D* **72**, 014002 (2005), arXiv:hep-ph/0503273.
 - [7] S. Clymton and H.-C. Kim, *Phys. Rev. D* **106**, 114015 (2022), arXiv:2208.04124 [hep-ph].
 - [8] H. Nagahiro, K. Nawa, S. Ozaki, D. Jido, and A. Hosaka, *Phys. Rev. D* **83**, 111504 (2011), arXiv:1101.3623 [hep-ph].
 - [9] M. A. Abolins, R. L. Lander, W. A. W. Mehlhop, N. huu Xuong, and P. M. Yager, *Phys. Rev. Lett.* **11**, 381 (1963).
 - [10] U. Karshon, G. Mikenberg, Y. Eisenberg, S. Pitluck, E. E. Ronat, A. Shapira, and G. Yekutieli, *Phys. Rev. D* **10**, 3608 (1974).
 - [11] V. Chaloupka, A. Ferrando, M. J. Losty, and L. Montanet, *Phys. Lett. B* **51**, 407 (1974).
 - [12] R. Gessaroli *et al.*, *Nucl. Phys. B* **126**, 382 (1977).
 - [13] C. Evangelista *et al.*, *Nucl. Phys. B* **178**, 197 (1981), [Erratum: *Nucl.Phys.B* 186, 594 (1981), Erratum: *Nucl.Phys.A* 435, 859-859 (1985)].
 - [14] M. Atkinson *et al.* (Omega Photon), *Nucl. Phys. B* **243**, 1 (1984).
 - [15] M. Atkinson *et al.* (Omega Photon), *Phys. Lett. B* **138**, 459 (1984).
 - [16] B. Collick *et al.*, *Phys. Rev. Lett.* **53**, 2374 (1984).
 - [17] S. Fukui *et al.*, *Phys. Lett. B* **257**, 241 (1991).
 - [18] A. Alde *et al.* (IHEP-IISN-LANL-LAPP-KEK), *Z. Phys. C* **54**, 553 (1992).
 - [19] P. Weidenauer *et al.* (ASTERIX), *Z. Phys. C* **59**, 387 (1993).
 - [20] J. A. Oller and U. G. Meissner, *Phys. Lett. B* **500**, 263 (2001), arXiv:hep-ph/0011146.
 - [21] D. Jido, J. A. Oller, E. Oset, A. Ramos, and U. G. Meissner, *Nucl. Phys. A* **725**, 181 (2003), arXiv:nucl-th/0303062.
 - [22] M. Albaladejo, P. Fernandez-Soler, F.-K. Guo, and J. Nieves, *Phys. Lett. B* **767**, 465 (2017), arXiv:1610.06727 [hep-ph].
 - [23] U.-G. Meißner, *Symmetry* **12**, 981 (2020), arXiv:2005.06909 [hep-ph].
 - [24] R. Blankenbecler and R. Sugar, *Phys. Rev.* **142**, 1051 (1966).
 - [25] R. Aaron, R. D. Amado, and J. E. Young, *Phys. Rev.* **174**, 2022 (1968).
 - [26] M. Bando, T. Kugo, S. Uehara, K. Yamawaki, and T. Yanagida, *Phys. Rev. Lett.* **54**, 1215 (1985).
 - [27] M. Bando, T. Kugo, and K. Yamawaki, *Nucl. Phys. B* **259**, 493 (1985).
 - [28] G. Janssen, K. Holinde, and J. Speth, *Phys. Rev. C* **49**, 2763 (1994).
 - [29] J.-Y. Kim and H.-C. Kim, *Phys. Rev. D* **97**, 114009 (2018), arXiv:1803.04069 [hep-ph].
 - [30] J.-Y. Kim, H.-C. Kim, G.-S. Yang, and M. Oka, *Phys. Rev. D* **103**, 074025 (2021), arXiv:2101.10653 [hep-ph].
 - [31] M. I. Haftel and F. Tabakin, *Nucl. Phys. A* **158**, 1 (1970).
 - [32] R. Machleidt, K. Holinde, and C. Elster, *Phys. Rept.* **149**, 1 (1987).
 - [33] K. W. Edwards *et al.* (CLEO), *Phys. Rev. D* **61**, 072003 (2000), arXiv:hep-ex/9908024.
 - [34] A. J. Woss, C. E. Thomas, J. J. Dudek, R. G. Edwards, and D. J. Wilson, *Phys. Rev. D* **100**, 054506 (2019), arXiv:1904.04136 [hep-lat].
 - [35] E. E. Kolomeitsev and M. F. M. Lutz, *Phys. Lett. B* **582**, 39 (2004), arXiv:hep-ph/0307133.
 - [36] L. S. Geng, E. Oset, L. Roca, and J. A. Oller, *Phys. Rev. D* **75**, 014017 (2007), arXiv:hep-ph/0610217.
 - [37] S.-i. Nam, *Phys. Rev. D* **96**, 076021 (2017), arXiv:1706.05521 [hep-ph].